Dynamics of the $N(^4S)+NO(X\,^2\Pi)\rightarrow N_2(X\,^1\Sigma_g^+)+O(^3P)$ atmospheric reaction on the $^3A''$ ground potential energy surface. III. Quantum dynamical study and comparison with quasiclassical and experimental results

Antonio Aguilar, Miquel Gilibert, Xavier Giménez, Miguel González, and R. Sayós
Departament de Química Física, Facultat de Química, Universitat de Barcelona, Martí i Franquès, 1, 08028 Barcelona, Spain

A detailed reactive–infinite-order sudden approximation (R-IOSA) study of the reactivity of the $N+NO\rightarrow N_2+O$ system has been carried out in the 0.0038 to 1.388 eV translational energy range and the results have been compared with the existing quasiclassical trajectory (QCT) and experimental data available. The general features already observed in the previous QCT studies are reproduced qualitatively in the quantum study, even though some differences arise in the product vibrational distributions and state-to-state opacity functions in the low energy range. The observed differences have been justified in terms of the anisotropy of the potential energy surface and the vibrational barriers to reaction at fixed angles. A strong vibrational adiabaticity is observed quantally in the low translational energy range, disappearing at moderately high collision energies (around 0.3 eV), where a simple Franck–Condon type model is capable of describing the evolution of the vibrational distribution with translational energy. The vibrational distributions at fixed angles have been discussed within the context of Polanyi's and Light's correlation between products vibrational excitation and the features of the potential energy surface. The validity of extending the conclusions drawn from collinear to three-dimensional (3D) collisions is discussed. Finally, the detailed reaction mechanism is examined in light of the vibrational matrix elements of the close-coupling interaction matrix. © *1995 American Institute of Physics.*

I. INTRODUCTION

Although the N atom is the most abundant element in earth's atmosphere and in spite of its prominence in atmospheric chemistry, relatively few direct measurements of the reaction process of this species have been reported. In particular, the reaction of ground state $N(^4S)$ atoms:[1]

$$N(^4S)+NO(X\,^2\Pi)\rightarrow N_2(X\,^1\Sigma_g^+)+O(^3P),$$
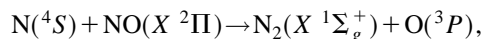
$$\Delta H_{298}^0=-74.95\quad\text{kcal mol}^{-1}\qquad(1)$$

has been used as a titrant for nitrogen atoms in low pressure discharge flow systems[2] and is thought to act as a sink for NO molecules at altitudes above 40 km.[3]

A great majority of the experimental studies report only rate constants, with no information about the detailed dynamical microscopical mechanism of this reaction. Many experimental techniques have been employed to determine the value and temperature dependence of the rate constant for this reaction. Thus Kistiakowsky and Volpi[4] gave a lower bound for the absolute rate constant k at 298 K (4.0×10^{11} cm³/mol s) using a discharge flow system with mass spectrometric measurement of products. Other measurements refer to the rate constant dependence on T between 196 and 700 K[5–11] and between 1251 and 3152 K.[12,13] It was proposed that this behavior can be well represented by a constant value of $(2.11\pm0.66)\times10^{13}$ cm³/mol s between 196 and 3150 K.[13] Most of this data are in good agreement with the recommended value of $(1.6\pm0.3)\times10^{13}$ cm³/mol s reported by Baulch *et al.*[14] The main conclusion that can be drawn from these measurements is that this reaction proceeds with very little or no energy barrier. The highest experimental estimate is 0.82 kcal/mol, whereas other authors claim that this reaction should proceed with no activation energy. This assumption has been subsequently confirmed by the contracted CI (CCI) calculations of Walch and Jaffe,[15] who found an energy barrier of only 0.5 kcal/mol on the ground $^3A''$ potential energy surface (PES). These same authors report a 14.4 kcal/mol energy barrier for the $^3A'$ excited PES connecting reactants and products in their ground electronic states and therefore, the ground potential energy surface is adequate to describe reactivity at room temperatures and in the moderate translational energy range.

In our two previous works on this system we undertook to build an accurate analytical PES using the Sorbie–Murrell many-body expansion[16] to carry out a study of the dynamics of this system on the ground PES. The procedure and preliminary analysis of the dynamical features were reported in paper I of this series,[17] whereas paper II was devoted to a detailed quasiclassical trajectory study of the dynamical properties of this system.[18] On this analytical PES, the incoming N atom reaches the saddle point for $R_{NN}=2.28$ Å, $R_{NO}=1.15$ Å and $\theta_{NNO}=107.10°$ (which is equivalent to a Jacobi angle of 126°), falling subsequently to products.[17,18] The bending potential around the saddle point configuration shows a smooth evolution from a repulsive behavior at 180° (0.75 eV above the saddle point energy) to an attractive configuration at the saddle point NNO angle and then again rising steeply for bent angles (0.84 eV at 80°).

In addition to the fact that reactivity is observed over the whole energy range scanned (from 0.01 to 1.8 eV) because of the lack of barrier on the fitted PES, the main conclusion that can be drawn from these studies is the strong influence

of the repulsive part of the potential in determining the outcome of reaction. Also, the quasiclassical trajectories (QCT) rate constants and fraction of available energy being disposed of as vibration agree reasonably well with the experimental existing results.[14,19,20] From these studies a change in the shape of the vibrational distribution in products ($P(v')$) with energy is observed, going from a distribution peaking at $v'=2-3$ at low translational energies to a smoothly decreasing distribution in the high energy range. This fact was subsequently interpreted in terms of the direct mechanism for this reaction and the shape of the reaction window at each energy. The strong anisotropy of the potential together with the fact that almost all reactive trajectories are well controlled by the bending potential around the saddle point prompted the application of the angle dependent line-of-centers (ADLOC) model to this reaction with good agreement between the model predictions and the QCT data.[21] Some of the spirit of the ADLOC application will be used later on regarding the analysis of the angle-dependent reactivity.

As stated above, an important factor in describing and interpreting the reactivity of the N and NO species in the upper atmosphere is the shape of the vibrational distribution in products, since most reactions take place under nonequilibrium conditions. Population deviations from statistical predictions of product vibrational states is a peculiar feature singled out previously.[22] More recently, similar results have been found out in other exothermic atmospheric processes,[23] as well as that the quantum and classical results in this respect can differ significantly. This has also been observed in other important combustion and laser precursor[24] processes. On the other hand, the quantum mechanical methods usually employed in reactive scattering can furnish state-to-state properties without the limitations associated with the QCT method in what regards the assignment of the product quantum states. Therefore, even though, to the best of our knowledge, no experimental detailed dynamical information has been so far reported in the literature, we have thought it interesting to carry out a quantum dynamical study of this system, which will enable us to characterize also all the other dynamical properties of interest.

Since the PES for this reaction shows no electronic barrier to reaction, this work could be carried out in principle by means of the quantum capture theory,[25–27] which considers only the long range part of the potential in the entrance channel to calculate accurately integral cross sections and rate constants. However, two important features prevent the application of this model to the title reaction. First, the method cannot provide state-to-state quantities since they are obtained summed over all product states, and second and more important, the method is unapplicable as originally formulated to reaction paths evolving through configurations more open or bent than that of the saddle point, since an electronic barrier appears. As it will be seen, the contribution of these configurations to reactivity is by no means negligible. On the other hand, even though rigorous quantum 3D methods have been greatly improved in the last 6–8 years,[28] both from the methodological and computational point of view, the highly exothermicity of this system and the great number of rovi-brational states required for close-coupling calculations to be carried out under convergence conditions make it very difficult to undertake such a study free of restrictions which reduce the dimensionality of the coupled set of differential equations. Thus, for instance, in the F+H$_2$ system, a total of 150 rovibrational states for each of the 31 total angular momentum partial waves is required to get fully converged *integral cross sections* from close-coupling calculations,[29] whereas a similar study with N+NO would need about 1500 states for each of 200 partial waves to ensure convergence. Then, a detailed investigation of the reaction dynamics at a relatively low cost can only be performed by means of approximate methods. The reactive–infinite-order sudden approximation (R–IOSA) method[30–32] has been proven to be a reasonable, reliable and computationally cheap way of calculating dynamical properties of interest and so it has been chosen to carry out this study.

This paper is organized as follows: In Sec. II we give details of the methods and calculations performed. In Sec. III we present the results with a detailed comparison between QCT and R–IOSA dynamical properties and wherever possible with experimental data. Finally, Secs. IV and V are devoted to the discussion of the results and the main conclusions of this study.

II. METHODOLOGY AND COMPUTATIONAL DETAILS

Calculations have been performed by means of the same R–IOSA procedure used in previous works,[30–32] so only a scheme of the practical steps needed will be outlined. The calculation is divided in two main parts. In the first part the potential energy, vibrational functions and overlaps are computed for each sector into which the configuration space is divided. In the second part, the solution is propagated through the sectors to get the fixed angle S-matrix elements for all relevant values of the orbital angular momentum at each desired collision energy. These two steps are repeated at each relevant (non-negligibly contributing to reactivity) collision Jacobi atom–diatom orientation angle (γ). At this point, it has to be noted that this angle must not be mistaken by the attack angle γ (180° minus the ABC bond angle) employed in the previous ADLOC study of this system.[21] The Jacobi angle provides a better description of the process, because it eliminates possible ambiguities caused by taking γ as defined in Ref. 21 enabling also a better comparison with the R–IOSA results.

Configuration space has been divided into 500 sectors (250 for each reaction channel). For the energy range of interest, convergence within a few percent was obtained using 43 vibrational basis functions. The matching B parameter[32] is chosen automatically by means of a pseudoiterative procedure[33] and ranges from 0.85 to 0.97 depending on the collision angle considered. Propagation through the sectors is performed by means of the well-known R-matrix method of Light and Walker.[34] Circular collision coordinates are used, which are a good choice given the large value of the collinear skew angle (59.3°). The scanned translational energy E_T ranged from 0.0038 to 1.49 eV with a total of 19 different values. The NO rotational quantum number was fixed to $j=7$ (the most populated j level for $v=0$ at 300 K)

throughout all the calculations. For each energy value, a total of 21 collision angles were included, ranging from 80° to 180° in steps of 5°. For each collision angle and energy, all angular momentum partial waves necessary for integral cross section convergence were included, the maximum number (l_{max}) required being 188 at $E_T = 1.49$ eV and $\gamma = 145°$. With these parameters, the first part (computation of the potential energy, vibrational functions and overlaps) lasted an average of 80 s on an IBM 3090/600J computer, while the computation of a fixed angle cross section needed up to 4000 s on the same computer, at the highest energies.

All calculations have been carried out assuming the following transformation between reactants and products orbital and rotational angular momenta:

$$l \rightarrow l', \quad j \rightarrow j',$$

which has been based in previous QCT calculations.[17,18]

Solving the Schrödinger equation, under R–IOSA restrictions, provides the S-matrix elements $S_{vv'}^l(E_T, \gamma)$, where v and v' are reactant and product vibrational quantum numbers, l is the reactants orbital angular momentum quantum number and γ is the reactants Jacobi atom–diatom orientation angle. A state-to-state analysis of the reactivity may start by a less averaged quantity, the fixed angle opacity function, which is simply the squared modulus of the corresponding S-matrix element when plotted vs the orbital angular momentum quantum number. The first sums over this quantity give rise to specific opacity functions (γ averaging) or steric factors (l averaging):

$$P_{vv'}^l(E_T) = \frac{1}{2} \int_{-1}^{1} |S_{vv'}^l(E_T, \gamma)|^2 d\cos\gamma \tag{2}$$

and

$$\sigma_{vv'}^\gamma(E_T) = \frac{\pi}{k_{vj}^2} \sum_{l=0}^{\infty} (2l+1)|S_{vv'}^l(E_T, \gamma)|^2. \tag{3}$$

The usual differential cross section is expressed in terms of products of S-matrix elements times Legendre polynomials $P_l(\cos\theta)$, where θ is the scattering angle, in the form

$$\frac{d\sigma_{vv'}(E_T)}{d\Omega} = \frac{1}{4k_{vj}^2} \sum_{l=0}^{\infty} \sum_{l'=0}^{\infty} (2l+1)(2l'+1)P_l(\cos\theta)$$

$$\times P_{l'}(\cos\theta)\frac{1}{2} \int_{-1}^{1} S_{vv'}^{l*}(E_T, \gamma)$$

$$\times S_{vv'}^{l'}(E_T, \gamma)d\cos\gamma \tag{4}$$

allowing the averaging procedure over the scattering polar and azimuthal angles to be continued to derive the R–IOSA integral cross section:

$$\sigma_{vv'}(E_T) = \frac{\pi}{k_{vj}^2} \sum_{l=0}^{\infty} (2l+1)\frac{1}{2}$$

$$\times \int_{-1}^{1} |S_{vv'}^l(E_T, \gamma)|^2 d\cos\gamma, \tag{5}$$

where (5) is in turn obtainable, within the R–IOSA context, in a straightforward manner from a direct integration over $\cos(\gamma)$ of Eq. (3).

The QCT 3D calculations have been carried out using the TRIQCT program.[35] The integration methods and Monte Carlo sampling procedures have been described elsewhere.[36] Trajectories were computed for E_T ranging from 0.01 to 1.8 eV, with the NO molecule placed in the $v = 0$, $j = 7$ rovibrational level. All of these conditions had already been reported in our previous works,[17,18,21] but we carried out additional trajectories in order to improve statistics so as to compare with the R–IOSA state-to-state dynamical magnitudes. In all, about 180 000 additional trajectories were integrated taking an average of 13 s per trajectory on both the IBM 3090/VF 600J and an HP Apollo 735GRX Workstation.

To compare the classical and quantum results, we had to carry out some very simple transformations. The angle-dependent partial cross sections as a function of the Jacobi angle [the classical quantity equivalent to expression (3)] were built by recording and classifying reactive trajectories in bins of $\Delta\cos(\gamma) = 0.1$ at several distances between N and the center of mass of NO (see Sec. III B). In order for Monte Carlo sampling to be done properly, we checked that the total number of trajectories followed a uniform distribution in $\cos\gamma$ at the beginning of the trajectories (large Jacobi R distances). Thus, the classical expression analogous to (3), summed over v' at fixed v and j, is

$$\sigma_v^\gamma = \pi b_{max}^2 \frac{N_R(v,j,E_T,\cos(\gamma))}{N_T(v,j,E_T)\Delta\cos(\gamma)}, \tag{6}$$

where b_{max} is the maximum impact parameter leading to reaction. For NO in the initial (v,j) rovibrational state, $N_T(v,j,E_T)$ is the total number of trajectories with energy E_T and $N_R(v,j,E_T,\cos(\gamma))$ is the number of reactive trajectories between $\cos(\gamma)$ and $\cos(\gamma)+\Delta\cos(\gamma)$, with $\Delta\cos(\gamma)$ the length of the binning interval (0.1).

For the opacity functions analogous to (2), we carried out trajectory calculations considering a uniform distribution between 0 and b_{max}. The resulting reactive trajectories were then classified according to their final v' value in order to obtain the state-to-state classical property. The sum over v' gives the total opacity function. To make comparison between classical and quantum results easier, we have transformed the 0–b_{max} interval to the equivalent 0–l_{max} range according to the equation

$$\{l(l+1)\}^{1/2}\hbar = \mu v b, \tag{7}$$

where μ is the reactants reduced mass and v is the relative velocity.

Finally, for the differential cross section of expression (4), summed over all v', the classical analog runs like

$$\frac{d\sigma_v}{d\Omega} = \pi b_{max}^2 \frac{N_R(v,j,E_T,\theta)}{N_T(v,j,E_T)2\pi\sin(\theta)\Delta\theta}. \tag{8}$$

To compare the R–IOSA and QCT data with the experimental findings, the rate coefficient defined as

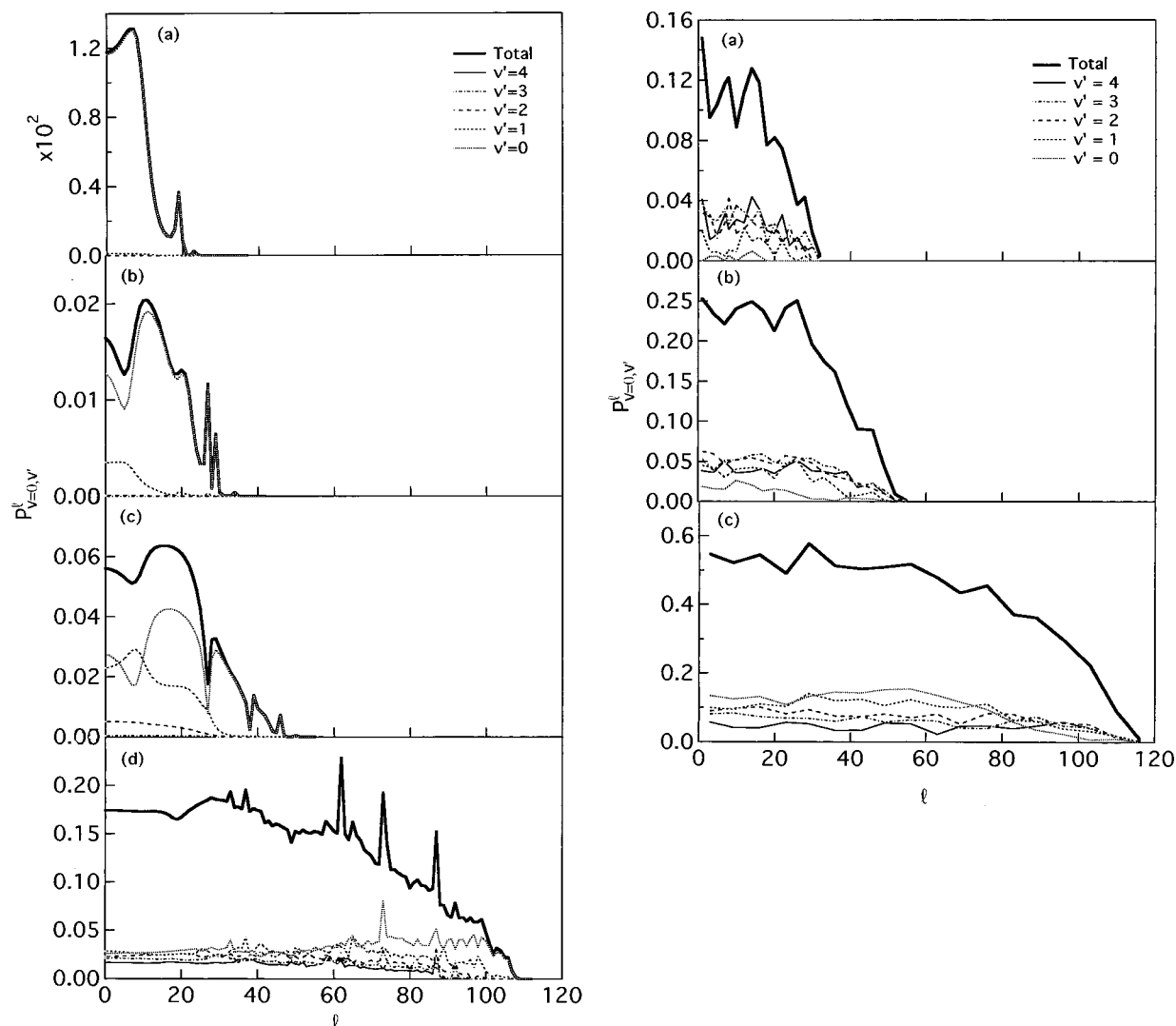FIG. 1. State-to-state and total R–IOSA (left) and QCT (right) opacity functions for N+NO($v=0$, $j=7$), at several translational energies. R–IOSA results: (a) 0.0178, (b) 0.0388, (c) 0.0882, and (d) 0.488 eV. QCT results: (a) 0.0388, (b) 0.1, and (c) 0.5 eV.

$$k_v(T) = \left(\frac{8k_B T}{\pi \mu_{\mathrm{N,NO}}}\right)^{1/2} \left(\frac{1}{k_B T}\right)^2 \int_0^\infty E_T \sigma_v(E_T)$$

$$\times \exp\left\{-\frac{E_T}{k_B T}\right\} dE_T \qquad (9)$$

was also calculated, where $\sigma_v(E_T) = \Sigma_{v'} \sigma_{vv'}(E_T)$ and k_B is the Boltzmann constant.

III. RESULTS

A. Opacity functions

The R–IOSA and QCT opacity function ($P_{v=0,v'}^l$) plots at several E_T values, with NO in the ground vibrational state, are presented in Fig. 1. On the overall, the behavior of the curves is the one to be expected in most systems, with reactivity being a decreasing function of the orbital angular momentum l. The most interesting features of the R–IOSA results are the presence of peaks over the whole energy range, the high vibrational adiabaticity of the opacity function at low translational energies and the fact that for all E_T values

explored at high l values the dominant transition is that corresponding to $v=0 \rightarrow v'=0$. On the other hand, the classical results display a similar behavior, even though in this case no peaks are observed (the differences in the reaction probability at different l values may be attributed in most cases to statistical uncertainties, hence the form at high E_T is smother). In this case, differently from the quantum results, the dominant state-to-state contribution to the opacity function at low energies is not the $v=0 \rightarrow v'=0$ one. Another marked difference between the quantum and classical distribution is the absolute magnitude of the opacity function, with quantum values usually much lower than the classical ones. The l value range contributing to reactivity is very similar in both cases, however. Given the strong anisotropy of the potential energy surface of this system,[18] the differences in the absolute magnitudes are not surprising since the R–IOSA method does not allow for reorientation to take place, even though, as it will be shown below, many other QCT and quantum dynamical results fit each other reasonably well. For instance, leaving apart the sharp peaks appear-
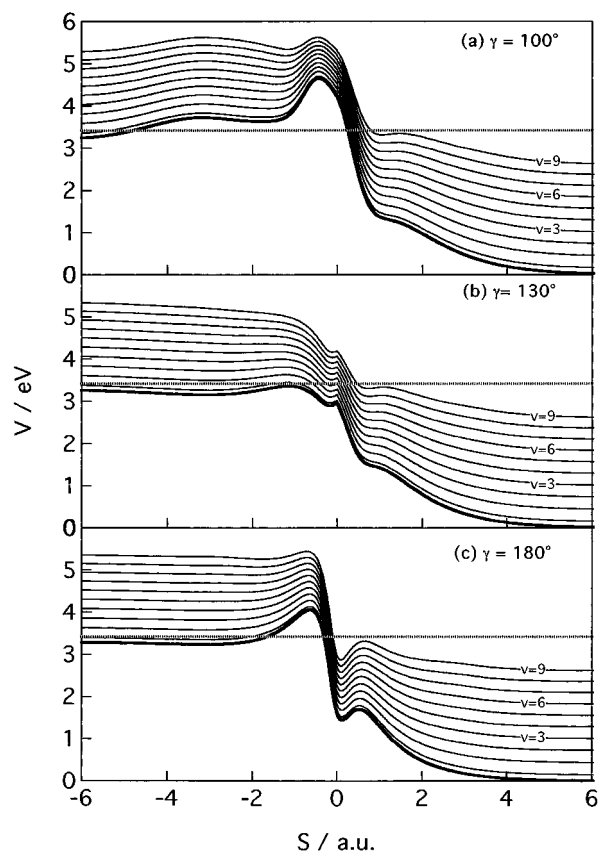
FIG. 2. Vibrational adiabatic curves along the reaction coordinate (the translational coordinate of the circular collision coordinate system, see text for its meaning) for several NNO fixed orientation angles: (a) 100°, (b) 130°, and (c) 180°. The straight line on each graphic indicates the asymptotic rovibrational energy of the N+NO($v=0$, $j=7$) reactants (3.4202 eV).

ing in the quantum results, the shapes of the overall opacity functions become increasingly similar as energy grows, which is consequent with the increasing sudden character of reaction dynamics as E_T grows.

The existence of sharp peaks in the opacity functions is usually understood in terms of the vibrational adiabatic paths along an adequate reaction coordinate.[37] These are shown for the N+NO system in Fig. 2, along with the ground potential energy curve. In the figure, the fixed-angle vibrational eigenvalues within each sector for all sectors and arrangement channels are plotted against the translational circular coordinate S[34] (defined in terms of mass-scaled Jacobi coordinates), with negative values designing reactant configurations and positive ones corresponding to products. For clarity, a straight line showing the reactants asymptotic rovibrational energy ($v=0$, $j=7$) has been added. The curves for $\gamma=130°$ approximately correspond to the saddle point configuration. It may be seen that at this angle there is no barrier to reaction although, as the angle is increased or decreased, a barrier appears, as reflected in the curves of Fig. 2. Another interesting feature is the presence of a very shallow minimum in the reactants zone and also after the saddle point for several γ angles. The appearance of sharp reactivity peaks is usually attributed to the discrete levels supported by these minima. However, when discussing the structure in the opacity function the centrifugal barriers due to nonzero orbital

angular momentum have to be taken into consideration. It may be the contribution of both these factors that leads to the appearance of peaks at selected energies and l values (see Fig. 1). On the other hand, the denser spectrum of reactivity peaks at high energy may be explained by the fact that, since as E_T is increased the range of l values contributing to reactivity is bigger so that more resonant conditions can be met.

The abovementioned minima on the potential energy surface were already reported in paper I of this series, and were found to cause no noticeable effect on reactivity from a classical point of view. It is also worth noting that, for all γ angles not negligibly contributing to reactivity at the energies explored in the present study, the sudden release of energy immediately after the saddle point is also reflected in a sharp fall of the adiabatic curves. The effect of these features on the reactivity will be analyzed below, in terms of interactions between vibrational states.

A distinct feature of the quantum opacity function is, in fact, the very strong vibrational adiabaticity observed below the average thermal energy (0.0388 eV). Thus, the almost exclusively dominant state-to-state opacity function at 0.007 78 eV is the 0→0 transition, whereas this same transition is responsible for the overall shape and magnitude of the $P^l_{v=0,v'}$ curve at 0.0388 eV. These results are rather surprising given the strong exothermic nature of this reaction (3.29 eV), which simply by energy conservation would allow levels up to $v'=12$ to be populated at thermal energies. Even though the vibrational adiabatic character is lost at higher energies, the 0→0 transition continues to be the dominant one over the whole energy range explored. Moreover, as evidenced in Fig. 1, there is an almost strict ordering of the state-to-state $P^l_{v=0,v'}$ curves over the whole l range. Thus, the $P^l_{v=0,v'}$ curves fall to zero for lower l values as v' increases. The classical state-to-state $P^l_{v=0,v'}$ curves show almost the same feature at high E_T (ca. 0.5 eV) even though not in the low energy range (0.0388 to 0.1 eV). As it will be shown below, these behaviors lead ultimately to a product vibrational inversion for the QCT data at low E_T and no inversion at high E_T, whereas no vibrational inversion is observed quantally over the whole energy range. The classical $P^l_{v=0,v'}$ plots show non-negligible probabilities for all v' values at high l. This contrasting behavior is not surprising since classical trajectories allow for angular momentum transfer between l and j' to occur and thus may modify the centrifugal barrier for a given initial l value. This is not allowed within the R–IOSA framework adopted for the present study because of the $l\rightarrow l'$ conservation. As mentioned in our previous studies, the potential energy surface for this system shows a marked anisotropy which may cause reorientation of the system along the collision and thus induces a change of l along a given trajectory.

The analysis of the R–IOSA state-to-state opacity function curves in Fig. 1 reveals other interesting facts. Whereas at low l values (or, equivalently, low impact parameters) and for sufficiently high energies there is a non-negligible contribution from the 0→v', $v'\neq0$, at the highest l values the dominant transition is that from 0→0. This behavior differs markedly from that observed in the at least formally similar
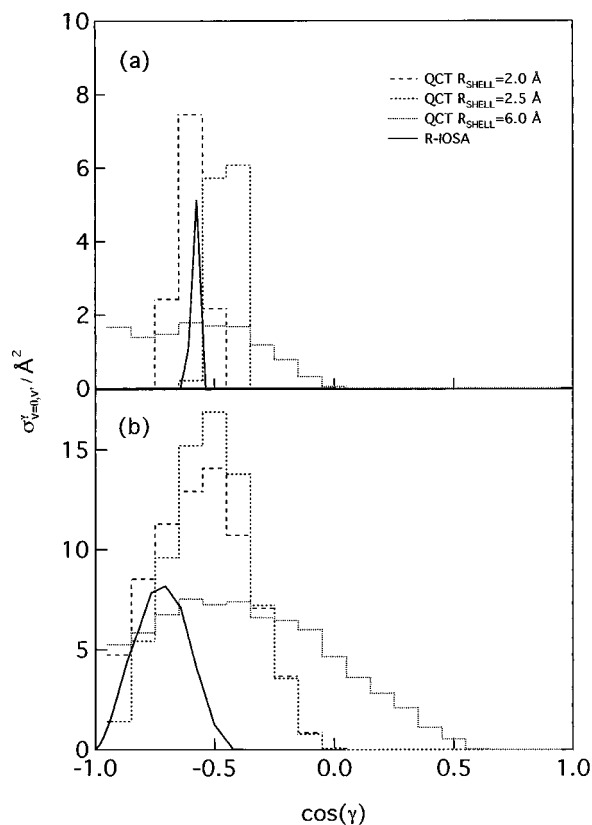
FIG. 3. Jacobi fixed-angle partial cross section. The R–IOSA results are superimposed on the QCT ones, drawn at different R_{shell} distances (see text): (a) $E_T=0.0388$ eV, (b) 0.788 eV.
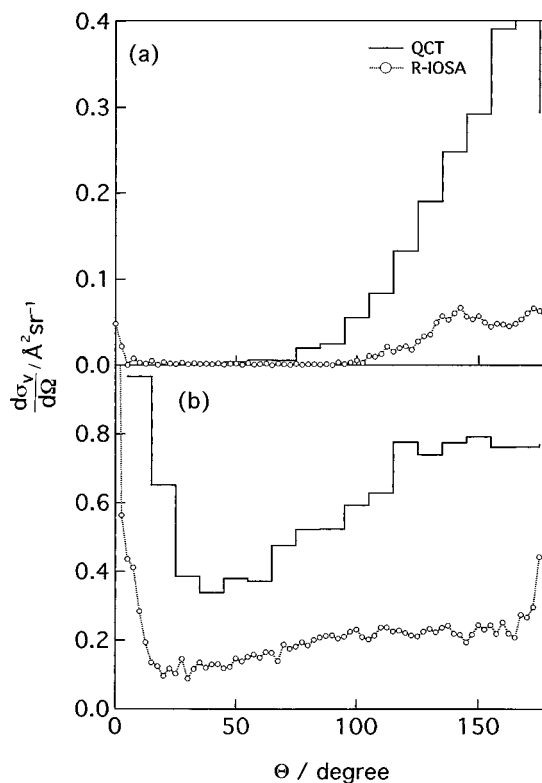

FIG. 4. QCT (continuous solid line) and R–IOSA (open circles, broken line) reactive differential cross sections at $E_T=0.0388$ (a) and 0.788 eV (b).

$N+O_2$ (Ref. 22) system, in which at low E_T the $0\rightarrow0$ transition was dominant at high l values but only minor at low angular momenta. In that study, a vibrational inversion was observed, which is not the case in the present quantum results.

B. Angle-dependent reaction cross section

Quantum and classical Jacobi angle-dependent partial cross sections [Eqs. (3) and (6)] are plotted as a function of the initial orientation angle in Fig. 3, at 0.0388 eV [3(a)] and 0.788 eV [3(b)] respectively. On both plots, the R–IOSA and QCT results are shown together. Although the QCT calculations have not been performed at fixed angle, we have kept track of the orientation angle at several Jacobi R distances (hereafter referred as R_{shell}). The $R_{shell}=6.0$ Å value corresponds to the starting point of each trajectory, $R_{shell}=2.5$ Å is the R distance at the saddle point configuration, and $R_{shell}=2.0$ Å shows results for a configuration after overcoming the saddle point.

The shape of the trajectory distribution at $R_{shell}=6.0$ Å is much broader than at $R_{shell}=2.5$ Å and lie completely within the $60°$–$180°$ and $90°$–$180°$ ranges, respectively, but of course the area under the curves is conserved. The exchange NO+N channel is very repulsive and is not open at the energies considered in the present study. The conservation of areas implies that all reactive trajectories must pass through $R_{shell}=2.5$ Å, i.e., near saddle point configurations, before

falling to products. It is interesting to remark that all trajectories reaching $R_{shell}=2.5$ and 2.0 Å become reactive.

The R–IOSA curve presents a much narrower angular window to reaction and a certain shift with respect to the classical results, even though, in general, both types of results tend to overlap at least partially. The quantum results tend to show a maximum at more open angles than the QCT ones. Thus, for $E_T=0.0388$ eV the maxima of the R–IOSA and QCT distributions are 125° and 116° respectively, while for $E_T=0.788$ eV they appear at 130° and 123°. An interesting point to remark here is the shift in the QCT $\sigma_{v=0,v'}^{\gamma}$ distribution at 2.0 Å that occurs in the low energy case and which is not observed at higher energies. This seems to indicate that there is still the possibility of some reorientation after the saddle point at low energies. On increasing energy, the mechanism becomes more direct.[17,18] The observed shift makes the maximum of the distribution to peak at 130°, thus increasing the contribution of more open configurations to the reaction window. In our previous QCT works[17,18] it was pointed out the existing correlation between open configurations and vibrational excitation, which may be an explanation for the vibrational inversion obtained at low energies, as opposed to the smoothly decreasing vibrational distribution observed at higher energies. As it will be shown below this correlation (which was first discovered by Blais and Truhlar)[38] has also been found in the R–IOSA quantum calculations, although with differences at the quantitative level.

The results for the reactive differential cross section are shown in Fig. 4. The agreement between classical and quantum results is very good from a qualitative point of view. The
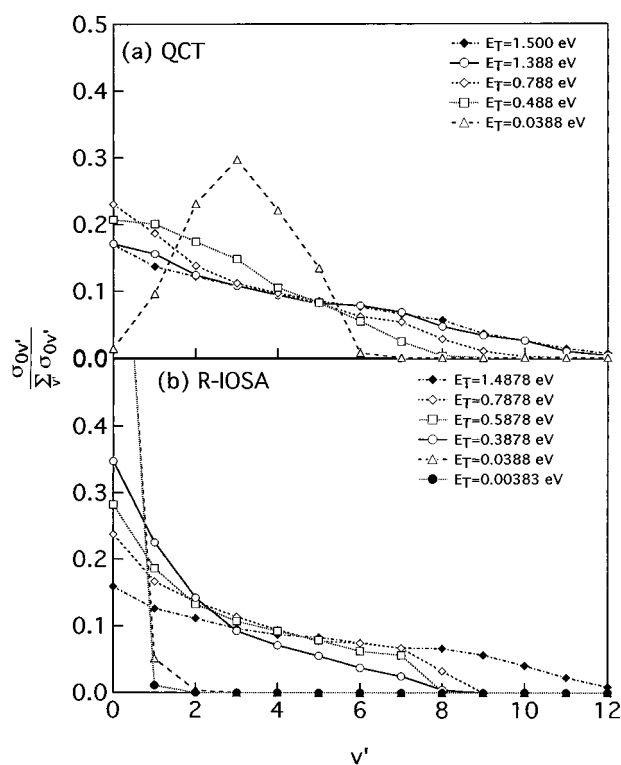
FIG. 5. Vibrational distributions of the N_2 molecules produced in the N+NO reaction, at several translational energies with NO in the $v=0$, $j=7$ rovibrational state. Figure 5(a) shows the QCT results and Fig. 5(b) the R–IOSA ones. The R–IOSA distributions for $E_T=0.003\,83$ and 0.0388 eV show probabilities close to 1 for $v'=0$.

main feature of these distributions is the marked backward character at low energies, which becomes more forward as energy is increased. As pointed out in our previous works on this system, the predominant backward scattering stems from the direct collision mechanism followed by this reaction. The agreement between quantum and classical results is in this case much better than that of the similar $N+O_2$ reaction.[22] It is also interesting to note that despite its underlying approximations the R–IOSA method is capable of furnishing a realistic description of the angular properties, even though, as it has been pointed out before, in this system the anisotropy of the potential is the main factor that determines the reaction outcome.

C. Product vibrational distributions

The vibrational distributions obtained at several energies are presented in Figs. 5(a) (classical) and 5(b) (quantum). The QCT results in Fig. 5(a) differ a bit from our previous results[17,18] due to the improved statistics for the calculations reported in the present work. The most striking difference between both types of results (classical and quantum) is the QCT vibrational inversion peaking at $v'=3$ obtained at $E_T=0.0388$ eV. As mentioned in our previous works on this system, this inversion disappears as translational energy is increased, giving rise to a monotonically decreasing shape which can be well described using a prior distribution.[18] This kind of behavior has been previously presented in the literature as one example of the disposal of excess energy over

and above that required to react.[39] By contrast, the R–IOSA distribution shows a much less complicated behavior as a function of energy. Over the whole energy range, a decreasing shape is found, even though at the higher energies explored the fall is much smoother than at low energies. Both types of distributions resemble each other, even quantitatively, in the high energy range. This is directly correlated with the convergence of the quantum R–IOSA collision to the QCT behavior as energy is increased, i.e., the system feels much less the potential and the collision are much better described within the fixed-angle approximation. Equivalently, it can be said that the range of configurations leading to reaction is vastly increased as E_T grows so that anisotropy effects are effectively reduced[18] and the system can be described within the prior vibrating rotor (VR) model assumptions, following the scheme of Levine *et al.*[40]

The fraction of available energy going into vibration of products (measured relative to the bottom of the potential) is 0.05 and 0.30 for the R–IOSA and QCT calculations, respectively, for average thermal ($T=300$ K) $E_T=0.0388$ eV. It can be seen that the agreement with the experimental fraction [0.28 ± 0.07 (Ref. 19) and 0.25 ± 0.03 (Ref. 20)] is poor for the quantum results and very good[17] for the classical ones. The difference lies in the strong adiabaticity observed in the quantum vibrational distribution, which is not accomplished at low energies by the classical treatment. As shown in our previous work[18] on this system, even though there is a strong reactant rotational dependence of the cross section, the fraction of vibrational energy in products estimated for NO($v=0$, $j=7$) is a good approximation to the thermally averaged quantity.

In our previous works[17,18,21] we explained the change in the shape of the QCT vibrational distribution by taking into account the correlation between the NNO angle at the saddle point and vibrational excitation of products. We concluded that due to the strong energy release after the saddle point, those configurations evolving with angles more open than that of the saddle point tended to give N_2 molecules in excited vibrational states, whereas the opposite happened for angles more bent than that of the saddle. The question is now whether quantally a similar mechanism can be observed. The best way we have found to check this point has been to plot the product vibrational distribution at different fixed angles at selected collision energies. The results of this analysis are given below.

D. Excitation function and rate constants

The QCT and R–IOSA integral cross sections for this system with NO($v=0$, $j=7$) are compared in Fig. 6. To enable a better comparison between the quantum and classical results, we have carried out additional quasiclassical trajectory calculations near threshold and also in the intermediate E_T range. This has in turn allowed for a better estimation of the QCT rate constant as compared with our previous values. The main feature of both distributions is the characteristically steep rise of the excitation function near threshold. However, the QCT curve rises in a much more abrupt way than the quantum one. The different behavior is more evident near threshold, where the quantum curve grows in a
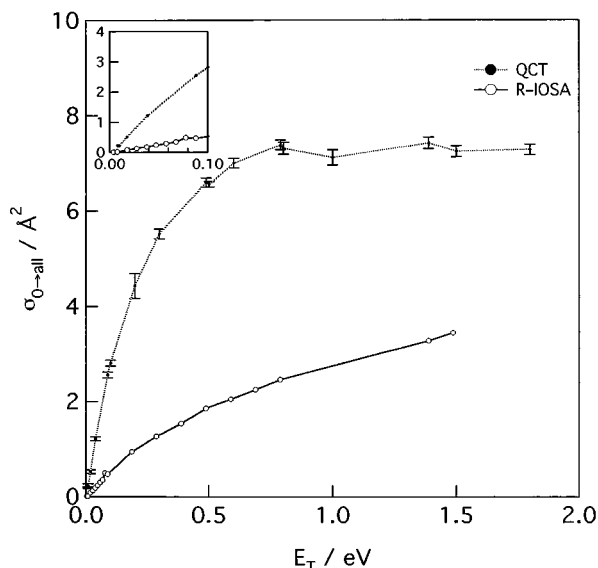
FIG. 6. Integral cross sections for the N+NO reaction, with NO in the $v=0$, $j=7$ state. Open circles: R–IOSA; full circles: QCT. The box embedded in the graph shows an enlarged picture of the threshold region (E_T between 0.0 and 0.1 eV, $\sigma_{0\rightarrow all}$ between 0.0 and 0.4 Å^2). Note the much smoother behavior for the quantum results in this region.

smoother way. As E_T is increased, the quantum results approach more the QCT ones, even though there is still a considerable difference in magnitude between both curves at the highest translational energy explored. All structures (peaks) found in the R–IOSA opacity functions disappear once integrated to give the total reactive cross section at each energy.

The differences between the QCT and R–IOSA excitation functions are usually attributed to the impossibility of the R–IOSA method to account for reorientation taking place during the collision process. As it has been shown in our previous works[17,18,21] the PES for this system is rather anisotropic, which means that reorientation may play an important role, justifying the differences observed. In fact, for the similar $N+O_2$ reaction, for which the PES is less anisotropic, a much more similar behavior of both excitation functions is observed.[22] Also, in the B+OH system, whose surface differs markedly from the present ones, the behavior of the integral cross section with energy follows a similar trend.[23] This seems to allow us to conclude that, in view of the experience gained in dealing with the R–IOSA application to triatomic systems, the R–IOSA cross sections are about half the classical analogs.

The QCT rate constants evaluated using expression (9) are 6.11×10^{12}, 1.34×10^{13}, and 1.94×10^{13} cm³/mol s at 300, 500, and 700 K, respectively, while the R–IOSA ones, evaluated using the same expression, are found to be 4.11×10^{11}, 1.48×10^{12}, and 3.18×10^{12} cm³/mol s respectively at the same temperatures. The QCT results differ a bit from our previously reported estimations due to the improved statistics obtained for the threshold region in the present calculations, but still when compared to the experimental results [$>4.0\times10^{11}$ (Ref. 4), $1.3\pm0.4\times10^{13}$ (Ref. 5), $1.5\pm0.8\times10^{13}$ (Ref. 6), $1.0\pm0.5\times10^{13}$ (Ref. 9), and $1.6\pm0.3\times10^{13}$ (Ref. 14) cm³/mol s at 300 K], they fall in general within the ex-

perimental error margin. The R–IOSA results however are usually from 15 to 6 times lower than the QCT and experimental values. As temperature increases, the differences become lower due to the larger contribution of the cross sections at higher translational energies where the quantum results differ less from the classical ones. At low temperatures, however, it is the region near threshold that plays an important role in determining the value of the rate constant. In this sense, the steeper rise of the QCT excitation function curve near threshold leads naturally to higher values of the rate constant than the comparatively smoother R–IOSA one, in good agreement with experiment.

IV. DISCUSSION

The form of the QCT and R–IOSA vibrational distributions stems directly from the contribution to reaction of the different state-to-state cross sections. As outlined in Sec. III, at moderately high collision energies (around 0.5 eV), the relative ordering of the different state-to-state $P_{v=0,v'}^{l}$ curves in the R–IOSA and QCT cases is similar. In particular it is noticed that at these energies, in the high l value region of the opacity function plot, a zone which by virtue of the weighing factor $2l+1$ plays an important role in determining the final value of the state-to-state cross sections, the dominant contribution comes from the 0 to 0′ transition. Leaving out the differences between classical and quantum curves arising from the imposition of l conservation (see above), the behavior is roughly similar in both cases. In this sense it is nice to observe how the quantum and classical results converge as collision energy is increased.

A. Angle-dependent vibrational distributions

The abovementioned convergence is also observed for more averaged quantities. For instance, the fractions of available energy in products from the R–IOSA calculations at $E_T=0.388$ and 0.788 eV are respectively 0.17 and 0.22, to be compared with the classical value of about 0.20 at these energies.[18] While being the expected result in the high energy range, where the details of the potential are in principle less important and the IOSA approximation is more valid, it is interesting in view of the behavior of the product vibrational distribution in the low and very low energy range (0.003 83 and 0.0388 eV). At these energies the quantum vibrational distributions show a sharp decrease from $v'=0$ with v' which is steeper for the lower E_T. Instead of that, a QCT vibrational inversion is observed at these very low energies. Thus, for the lowest translational energy explored in the QCT calculations, 0.007 887 eV, a vibrational inversion peaked at $v'=3$ is found. Only at moderately high collision energies does the classical vibrational distribution show a decreasing shape.

At these very low collision energies, the system should evolve as close as possible to the minimum energy reaction path. From the change of behavior found at higher energies, where the details of the potential are much less relevant for reactivity, it is clear that its shape and features are responsible for the observed differences at low energies. In this sense, even though the system proceeds with no barrier to-

ward products, we have checked the possibility that the ground vibrational state at the saddle point configuration might lie above the energy of reactants and thus give rise to tunneling. This would explain to some extent the observed discrepancies. Tunneling should not be expected to be important since all atoms are not lighter than N. Even though the zero point energy (ZPE) calculation has been carried out at fixed angle, within the R–IOSA scheme, thus not taking into account the ZPE bending energy, the real system should have an even higher barrier and thus the tunneling will be even less important. It is found that the ground vibrational state at the saddle point, which is also the point of highest effective potential, falls at 3.4078 eV, while the energy available for reaction [E_T plus the N+NO(v=0) asymptotic vibrational energy] at E_T=0.0388 eV is 3.4468 eV. Thus, even though by a very slight amount, the system has enough energy to overcome the vibrational barrier to reaction. The observed differences are likely to arise from the quite anisotropic character of the potential and the possibility that the system may experience reorientation along the trajectory. As seen on Fig. 3, the system leads only to reaction if it reaches the saddle point with an NNO angle within the open angular window. However, at these low energies (0.0388 eV) we have found in the QCT results that there is a subsequent reorientation of the system toward more open angles that those corresponding to the saddle point. Since, as shown in our previous work on this system,[17] open NNO angles correlate with vibrationally excited N$_2$ products, this would explain, at least partially, the differences observed with respect to the R–IOSA results, in which no reorientation is possible. Note also that, as evidenced in Fig. 3, this subsequent reorienting effect disappears at higher E_T, since the reaction mode becomes much more direct (sudden). Notice that the differential cross section plots become more forward with E_T as expected (the symmetry found at high translational energy (0.788 eV) is purely accidental [see Fig. 4(b)].

It is very interesting to ascertain whether in the R–IOSA calculations there is a similar correlation between the NNO Jacobi angle and the vibrational distribution in products [$P(v')=\sigma_{0v'}/\Sigma\sigma_{0v'}$]. To check this, we have plotted in Fig. 7 the $P(v')$ vs v' curves for different fixed NNO Jacobi angles at E_T=0.0388 eV and E_T=0.788 eV. Examination of the plots reveals a clear correlation between the NNO angle and the vibrational distribution in products, since relatively closed NNO angles (with respect to that of the saddle point) lead to sharply decreasing distributions and, as more open angles become reactive, the populations in excited v' levels become greater, eventually giving rise to a strong vibrational inversion (as much as v'=9 for γ=180°!). It is the compensating effects of the different angle-dependent vibrational distributions that give rise finally to the observed overall 3D vibrational distribution. At low energies, there is a very low weight of the open NNO angles, so that a strong decreasing distribution is observed [see Fig. 7(a)]. On increasing E_T, there is an ever greater contribution of the open NNO angular range, thus smoothing out the final $P(v')$ distribution.

The transition from a smoothly decreasing vibrational distribution to an inverted one occurs over a relatively narrow range of γ angles. Thus, at γ=130° a decreasing trend is
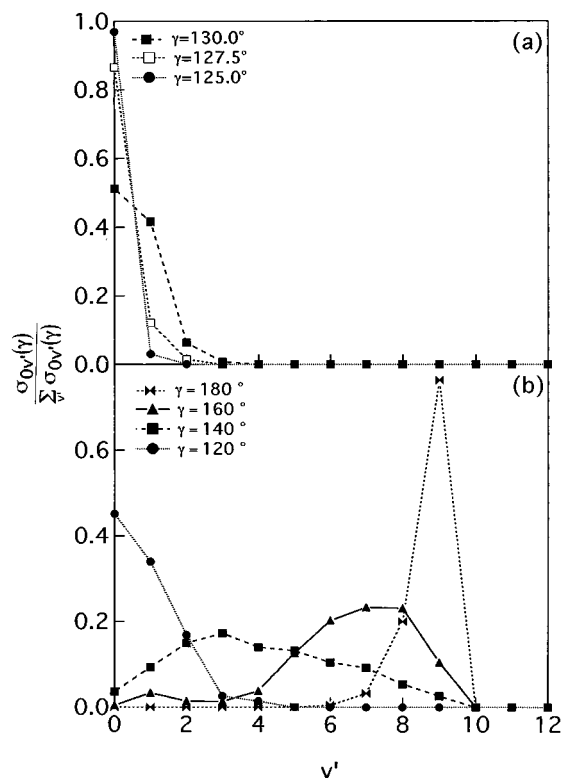

FIG. 7. Jacobi fixed angle R–IOSA N$_2$ vibrational distributions from N+NO for several NNO angles. (a) E_T=0.0388 eV, (b) E_T=0.788 eV. The vibrational distribution at each fixed angle has been normalized to unity.

obtained, while at γ=135° already a vibrational inversion can be found, especially at low energies. It is found that the barrier to reaction at γ=135° is 0.1416 eV, 0.2319 eV when considering the ground vibrational level (which includes the zero point energy of transition state and reactants). Thus, at E_T=0.0388 eV (0.1682 eV, total energy) the system can only cross the barrier at this angle through vibrational tunneling. Nevertheless, since trajectories do not take into account the zero point energy of the transition state, this angular range is classically open for reaction. Since these angles are the ones that lead to vibrational inversion and quantally the process has very low probability, it is clear that no vibrational inversion can be recovered when summing over the whole angular range. This effect is the more important in this energy range because of the steep rise in the cross section for small energy increments.

B. Franck–Condon model application

The considerable reactivity at high energies obtained in this system together with the direct collision mechanism and the sudden and repulsive energy release after the saddle point make the vibrational distributions of this system eligible to be interpreted in terms of the simple Franck–Condon (FC) model of Baer[41] and Laganà.[42] This model has been previously applied by us to the N+O$_2$ system[22] and the details can be found in that reference. Figure 8 shows the results of the model application for different values of the shifting parameter d, which is directly related with variations of collision energy. It can be seen that, as d increases, the vibrational
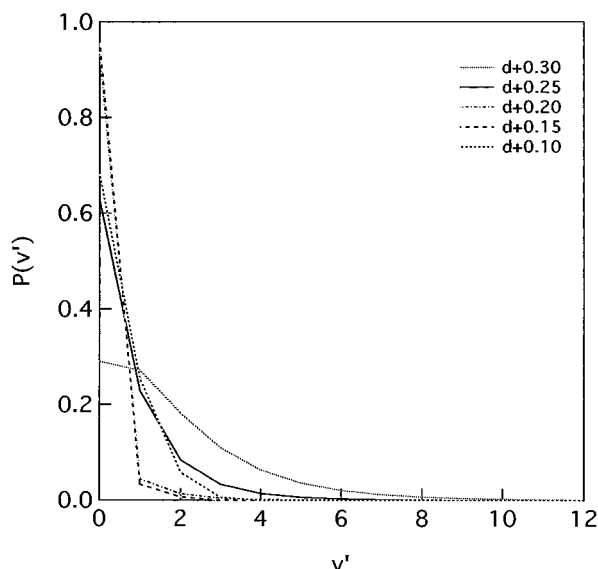
FIG. 8. N_2 vibrational distributions from N+NO obtained using the Franck–Condon model considering several shift parameters d (see text). Parameter d corresponds directly to overlapping the asymptotic N_2 and NO vibrational curves without shifting them one with respect to the other.

distribution evolves from a sharply decreasing shape to a smoother one, in a similar way as the R–IOSA distribution with energy (see Fig. 5). Note however that the dependence is not monotonous. Low d values show a behavior very similar to that obtained from R–IOSA calculations at the lowest E_T values considered. It may thus be concluded that the R–IOSA results are consistent with the FC behavior in the high energy range.

C. Vibrational adiabaticity in products

The vibrational adiabaticity in products observed in the quantum calculations reported in the present work is found to be directly correlated with the main features of the potential energy surface. Polanyi and co-workers[43] first, and afterwards Light and co-workers[44] carried out, in a series of works, a study of the factors that determine the vibrational energy release in products for collinear reactions. From the results of Polanyi,[43] it is implied that those surfaces having an early barrier to reaction tend to release energy in the direction of the forming diatomic bond (attractive energy release) and thus give rise to vibrational excitation in products, while for those surfaces having a late barrier, close to products, the energy is released mainly in the direction of the breaking diatomic bond, thus causing low vibrational excitation (repulsive energy release). Subsequently, Light *et al.*[44] gave a more quantitative formulation to the ideas outlined by Polanyi by studying the $H+Cl_2$ system employing a potential with variable parameters which lead to different types of potential energy surfaces. These authors found out that there are essentially three factors that govern the product energy release in a given reaction: the local kinetic energy along the translational coordinate u, the curvature of the reaction path and finally, the vibrational spacing and its variation with u. It is found that large force constants in the region of maximum

curvature, large radius of curvature (which means strongly skewed potentials) and low velocity make the system become increasingly adiabatic.

In our case, the symmetric stretching frequency at the saddle point is 1785 cm^{-1}, whereas it is 2359 cm^{-1} for N_2 and 1904 cm^{-1} for NO. This means that together with the sharp fall in energy after the saddle point, the NN force constant will increase with respect to the saddle value. Also, the angle-dependent skew angle[32] falls around 60° for the whole angular range. Even though important, this value does not suffice to characterize the system as having a large radius of curvature. Therefore, following the analysis of Polanyi[43] it seems the factor governing energy release at each angle is the more or less attractive character of the surface. As seen in Fig. 4 of Ref. 17, at a NNO angle of 110° it is not until both N come almost as close as the equilibrium bond distance of N_2 that the system falls down to products, giving rise to a rather repulsive energy release. This situation changes as the NNO angle opens up, since taking, for instance, 180° it may be seen that the fall and subsequent energy release in products starts relatively early after the saddle point configuration. This results in energy being partially released as the NN bond is formed. Putting it in terms of the Light *et al.*[44] analysis, for closed NNO angles the symmetric force constant is found to be similar to that of the N_2 products at the point of maximum curvature, thus giving rise to low vibrational excitation. Open NNO angles give rise to force constants, at the point of maximal curvature (the turning of the PES), more similar to that of the saddle point, thus favoring vibrational excitation.

The final vibrational distribution comes from the different distributions obtained at each angle after proper weighing. These can in turn be well accounted for using a "collinear-type" description of the surface at each angle to predict the type of energy release and the amount of adiabaticity expected, but in disagreement with Light's predictions[44] it seems rather unlikely that one can draw reliable conclusions about the 3D vibrational distribution in view of only the collinear case. It must also be stressed again that a full exact 3D study will have to be able to account for reorientation after the saddle point to extract a clear picture of the factors causing the vibrational distribution observed from QCT and experimental data, something which the R–IOSA method is only capable of doing partially.

D. Interaction matrix evolution through the reaction coordinate

The ultimate mechanism leading to the vibrational distribution obtained effectively must be accounted for by inspection of the off-diagonal terms in the interaction matrix which appears in the close-coupling equations, since the transitions between the different vibrational levels are governed mainly by those off-diagonal terms which couple the different translational functions $f(S_\lambda; i)$ within each sector i.[45] Close examination of these terms will lead to the knowledge of the detailed mechanism determining the vibrational distribution as well as the influence of the different zones of the PES in controlling the reactive vibrational transitions.

The system of equations to be solved, within the R–IOSA framework, is

$$\frac{d^2}{du_\lambda^2} \mathbf{f}(S_\lambda;i) = \mathbf{D}^{\lambda(i)}\mathbf{f}(S_\lambda;i) \tag{10}$$

where i refers to every sector. The symmetric matrix $\mathbf{D}^{\lambda(i)}$ is called the interaction matrix[45] and its elements are directly related to the probability of transition from a given initial vibrational state n_λ to a final vibrational state n_λ'. For the polar region, the expression of a matrix element is

$$\mathbf{D}_{n_\lambda n_\lambda'}^{\lambda(i)} = \left\langle \phi_{n_\lambda} \left| \eta_\lambda^2 \left[\frac{l_\lambda(l_\lambda+1)}{R_\lambda^2} + \frac{j_\lambda(j_\lambda+1)}{r_\lambda^2} \right] \right| \phi_{n_\lambda'} \right\rangle$$
$$+ \frac{2\mu_\lambda}{\hbar^2} \left[\frac{1}{2} (\epsilon_{n_\lambda j_\lambda} + \epsilon_{n_\lambda' j_\lambda}) - E \right] \langle \phi_{n_\lambda} | \eta_\lambda^2 | \phi_{n_\lambda'} \rangle$$
$$+ \frac{3}{4\sigma_\lambda^2} \delta_{n_\lambda n_\lambda'}, \tag{11}$$

whereas for the Cartesian region the following equation applies:

$$(\mathbf{D}^{\lambda(i)})_{n_\lambda n_\lambda'} = \left\langle \phi_{n_\lambda} \left| \frac{l_\lambda(l_\lambda+1)}{R_\lambda^2} + \frac{j_\lambda(j_\lambda+1)}{r_\lambda^2} \right| \phi_{n_\lambda'} \right\rangle$$
$$+ \frac{2\mu_\lambda}{\hbar^2} (\epsilon_{n_\lambda} - E) \delta_{n_\lambda n_\lambda'}. \tag{12}$$

Here η_λ is the curvature and is related to the transversal (vibrational) coordinate and the radius of the reference curve in the polar region. It is clear from expressions (11) and (12) that there are two types of contributions to the interaction matrix, one arising from the coupling through angular momentum terms (rotational as well as orbital) and the other from the coupling through the curvature. The second term will not change with l_λ or j_λ since it depends within each sector only on the form of the vibrational adiabatic eigenfunctions ϕ_{n_λ} and $\phi_{n_\lambda'}$, the curvature η_λ^2, and the difference between the energy eigenvalues of the two vibrational states n_λ and n_λ' and the total energy E. It is noticed that this term may become very important in the case of exothermic reactions. The first term in Eqs. (11) and (12) depends also on the values of the rotational and orbital angular momenta. In general, greater orbital or internal angular momenta will imply an increase of this term. Note also that, since l_λ and j_λ remain constant along a given calculation, this first term depends mainly on $1/R_\lambda^2$ and $1/r_\lambda^2$. On approaching the asymptotic region, the contribution of the orbital angular momentum part falls down to zero and only the term due to the internal angular momentum remains.

We have plotted in Fig. 9 the interaction matrix values vs the translational coordinate S for several reactive vibrational transitions at a translational energy of 0.788 eV, for a fixed NNO Jacobi angle of 160° and different values of the orbital angular momentum l. The plot is limited to the strong interaction region, since it is in this zone that the strongest couplings are to be expected. Superimposed on the figure is the potential energy curve as a function of S, as well as the first three vibrationally adiabatic potential energy curves. As the
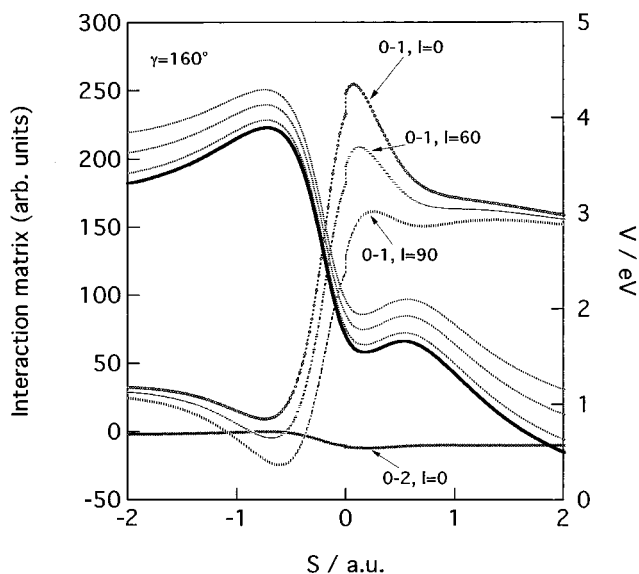

FIG. 9. Interaction matrix elements for N+NO at E_T=0.788 eV and a Jacobi fixed angle of 160° as a function of the translational circular coordinate S in arbitrary units. Only elements coupling v=0 and 1 and v=0 and 2 are shown, the higher couplings being negligibly small. The arrows indicate the different $v \rightarrow v'$ transitions for different values of the orbital momentum l. The right-hand side axis shows the potential energy value, which is also included in this figure as a function of S, with the thick line representing the electronic potential and the dotted lines the first three vibrational levels. Only the strong interaction region is shown.

system evolves from reactants (negative S) toward the barrier, the interaction matrix remains almost constant. Across the maximum, there is a slight fall of its value, only to be followed by a sharp rise in its value as the system is falling down to products. This confirms, from the reaction coordinate point of view, the behavior reported by Aquilanti,[46] in the sense that the highest nonadiabatic behavior is found near the so-called ridge region, or, equivalently, in those regions where the potential variation is higher. In addition, the plots corresponding to l=60 and l=90 illustrate also the influence of orbital angular momentum on each interaction element. In this case, we see a clear decrease of the coupling terms as l is increased. On the other hand, the nonadiabatic transitions involving more than one quanta are much less probable, as seen in the figure for the 0–2 element.

V. CONCLUDING REMARKS

In this work we have carried out a detailed R–IOSA study of the reactivity of the N+NO→N$_2$+O system with NO placed in the most populated rovibrational level at 300 K (v=0, j=7). The results have been compared with the previously existing and some new QCT data as well as with the experimental values available. The general dynamical features already described within the QCT framework have been reproduced, even though some quantitative differences have arisen due to strongly anisotropic character of the surface and the impossibility of the R–IOSA method to account for the reorientation thus induced.

The comparison between the initial Jacobi fixed angle cross sections with the QCT ones has shown that for this system reactivity is strongly conditioned by the reaction win-

dow around the saddle point configuration. Both quantum and classical differential cross sections are in reasonable agreement with each other and confirm the predominantly backward character of the reaction in the low energy range.

The vibrational distributions have been obtained for several energies and compared with QCT data. While at low energies the quantum results show no vibrational inversion, QCT data present a sharp inversion peaking at $v'=3$. The differences observed have been accounted for taking into account the reorienting effect of the surface after the saddle point at low energies as well as the fact that the vibrational adiabatic barriers cannot be incorporated into the classical treatment in an easy way. The correlation between vibrational excitation and Jacobi fixed angle observed previously in the QCT calculations has been confirmed in the R–IOSA ones. Application of the simple Franck–Condon model has led to a good agreement with the R–IOSA results.

The reason for the different vibrational distributions at fixed angles is explained using the criteria set forth by Polanyi *et al.* and Light *et al.* It is very difficult to predict the 3D behavior of the vibrational excitation using the same scheme as in the collinear case. Rather, the weight of the contribution for each orientation angle is found to determine the final vibrational distribution outcome. By inspecting the interaction matrix elements it is confirmed that the coupling changes sharply in the zone where the potential falls to products with the orbital angular momentum playing an important role.

ACKNOWLEDGMENTS

[1] M. Kh. Karapet'yants and M. L. Karapet'yants, *Thermodynamic Constants of Inorganic and Organic Compounds* (Ann Arbor–Humphrey Science, Ann Arbor, MI, 1970).

[2] H. I. Schiff, Ann. Geophys. **20**, 115 (1964).

[3] J. Heicklen and N. Cohen, Adv. Photochem. **5**, 157 (1968).

[4] G. B. Kistiakowsky and G. G. Volpi, J. Chem. Phys. **27**, 1141 (1957)

[5] L. F. Phillips and H. I. Schiff, J. Chem. Phys. **36**, 1509 (1962).

[6] M. A. A. Clyne and I. S. McDermid, J. Chem. Soc. Faraday Trans. **71**, 2189 (1975).

[7] J. H. Lee, J. V. Michael, W. A. Payne, and L. J. Stief, J. Chem. Phys. **69**, 3069 (1978).

[8] M. A. A. Clyne and B. A. Thrush, Proc. R. Soc. London, Ser. A **261**, 259 (1961).

[9] J. T. Herron, J. Chem. Phys. **61**, 35 (1978).

[10] Y. Takezaki and S. Mori, Bull. Inst. Chem. Res. Kyoto **45**, 388 (1967).

[11] C. L. Lin, D. A. Parker, and F. Kaufman, J. Chem. Phys. **53**, 3896 (1970).

[12] M. Koshi, M. Yoshimura, K. Fukuda, H. Matsui, K. Saito, M. Watanabe, A. Imamura, and C. Chen, J. Chem. Phys. **93**, 8703 (1990).

[13] J. V. Michael and K. P. Lim, J. Chem. Phys. **97**, 3228 (1992).

[14] D. L. Baulch, D. D. Drysdale, and D. G. Haine, *Evaluated Kinetic Data for High Temperature Reactions* (Butterworths, London, 1973), Vol. II.

[15] S. P. Walch and R. L. Jaffe, J. Chem. Phys. **86**, 6946 (1987); AIP Document No. PAPSJCPSA-**86**-6946-10.

[16] J. N. Murrell and K. S. Sorbie, J. Chem. Soc. Faraday Trans. II **70**, 1552 (1974); K. S. Sorbie and J. N. Murrell, Mol. Phys. **29**, 1378 (1975); J. N. Murrell, S. Carter, S. C. Farantos, P. Huxley, and A. C. J. Varandas, *Molecular Potential Energy Functions* (Wiley, New York, 1984).

[17] M. Gilibert, A. Aguilar, M. González, F. Mota, and R. Sayós, J. Chem. Phys. **97**, 5542 (1992).

[18] M. Gilibert, A. Aguilar, M. González, and R. Sayós, J. Chem. Phys. **99**, 1719 (1993).

[19] J. E. Morgan, L. F. Phillips, and H. I. Schiff, Discuss. Faraday Soc. **33**, 118 (1962).

[20] G. Black, R. L. Sharpless, and T. G. Slanger, J. Chem. Phys. **58**, 4792 (1973).

[21] R. Sayós, A. Aguilar, M. Gilibert, and M. González, J. Chem. Soc. Faraday Trans. **89**, 3223 (1993), and references therein.

[22] M. Baer, J. Chem. Phys. **60**, 1057 (1974); **62**, 4545 (1975); J. Phys. Chem. **85**, 3874 (1981); J. N. L. Connor, A. Laganà, J. C. Whitehead, W. Jakubetz, and J. Manz, Chem. Phys. Lett. **62**, 479 (1979); J. N. L. Connor, W. Jakubetz, A. Laganà, J. Manz, and J. C. Whitehead, Chem. Phys. **65**, 29 (1982); J. N. L. Connor, J. C. Whitehead, W. Jakubetz, and A. Laganà, Il Nuovo Cimento **63**, 116 (1985).

[23] M. Gilibert, X. Giménez, M. González, R. Sayós, and A. Aguilar, Chem. Phys. **191**, 1 (1995).

[24] A. Aguilar, M. Albertí, X. Giménez, X. Grande, and A. Laganà, Chem. Phys. Lett. **233**, 201 (1995); X. Giménez, J. M. Lucas, A. Aguilar, and A. Laganà, J. Phys. Chem. **97**, 8578 (1993); X. Grande, X. Giménez, M. Albertí, J. M. Lucas, and A. Aguilar (in preparation).

[25] D. C. Clary, Annu. Rev. Phys. Chem. **41**, 61 (1990).

[26] D. C. Clary, Mol. Phys. **53**, 3 (1984).

[27] D. C. Clary, Mol. Phys. **54**, 605 (1985).

[28] The work on rigorous quantum 3D methods has been recently reviewed in D. E. Manolopoulos and D. C. Clary, Annu. Rep. Progr. Chem. C **95**, (1989); W. H. Miller, Annu. Rev. Phys. Chem. **41**, 245 (1990); D. G. Truhlar, D. W. Schwenke, and D. J. Kouri, J. Phys. Chem. **94**, 7346 (1990); J.-M. Launay, in *Dynamical Processes in Molecular Physics*, edited by G. Delgado-Barrio (IOP, Bristol, 1993); *Advances in Molecular Vibrations and Collision Dynamics*, edited by J. M. Bowman (JAI, Greenwich, 1994), Vols. 2A and 2B.

[29] V. Khare, D. J. Kouri, and M. Baer, J. Chem. Phys. **71**, 1188 (1979); J. M. Bowman and K. T. Lee, *ibid.* **72**, 5071 (1980); D. G. Barg and D. Drohlshagen, Chem. Phys. **17**, 209 (1980); A. Laganà, X. Giménez, E. García, and O. Gervasi, Chem. Phys. Lett. **176**, 280 (1991); A. Laganà, A. Aguilar, X. Giménez, and J. M. Lucas, *ibid.* **189**, 138 (1992).

[30] A. Aguilar, X. Giménez, J. M. Lucas, O. Gervasi, and A. Laganà, Theor. Chim. Acta **79**, 191 (1991).

[31] A. Laganà, A. Aguilar, X. Giménez, and J. M. Lucas, J. Chem. Phys. **95**, 2218 (1991); Faraday Discuss. Chem. Soc. **91**, 121 (1991); in *Advances in Molecular Vibrations and Collision Dynamics,* edited by J. M. Bowman (JAI, Greenwich, 1994), Vol. 2A.

[32] H. Nakamura, A. Ohsaki, and M. Baer, J. Phys. Chem. **90**, 6176 (1986).

[33] X. Giménez, Ph.D. thesis, Universitat de Barcelona, Spain (1991).

[34] J. C. Light and R. B. Walker, J. Chem. Phys. **65**, 1598 (1976); **65**, 4272 (1976).

[35] M. Gilibert, M. González, and R. Sayós, TRIQCT Program (1992).

[36] M. González and R. Sayós, Chem. Phys. Lett. **164**, 643 (1989); M. González, A. Aguilar, and R. Sayós, Chem. Phys. **132**, 137 (1989); R. Sayós, M. González, and A. Aguilar, *ibid.* **141**, 402 (1990).

[37] D. G. Truhlar and A. Kuppermann, J. Chem. Phys. **52**, 3841 (1970); R. D. Levine and S. F. Wu, Chem. Phys. Lett. **11**, 557 (1971); J. M. Launay and M. LeDourneuf, J. Phys. B **15**, L455 (1982); B. C. Garrett and D. G. Truhlar, J. Phys. Chem. **86**, 1136 (1982); R. T. Skodje, D. W. Schwenke, D. G. Truhlar, and B. C. Garrett, *ibid.* **88**, 628 (1984); V. Aquilanti, S. Cavalli, G. Grossi, and A. Laganà, J. Mol. Struct. **107**, 95 (1984).

[38] N. C. Blais and D. G. Truhlar, Chem. Phys. Lett. **118**, 379 (1985).

[39] A. M. G. Ding, L. J. Kirsch, D. S. Perry, J. C. Polanyi, and J. L. Schreiber, Faraday Discuss. Chem. Soc. **55**, 252 (1973).

[40] R. B. Bernstein and R. D. Levine, J. Chem. Phys. **57**, 434 (1972); A. Ben-Shaul, R. D. Levine, and R. B. Bernstein, *ibid.* **57**, 5427 (1972).

[41] M. Baer, J. Phys. Chem. **85**, 3974 (1981).

[42] A. Laganà, J. Chem. Phys. **86**, 5523 (1987).

[43] J. C. Polanyi, Acc. Chem. Res. **5**, 161 (1972).

[44] C. C. Rankin and J. C. Light, J. Chem. Phys. **51**, 1701 (1969); G. Miller and J. C. Light, *ibid.* **54**, 1635 (1971); *ibid.* **54**, 1643 (1971); D. G. Truhlar and D. A. Dixon, in *Atom-Molecule Collision Theory: A Guide for the Experimentalist*, edited by R. B. Bernstein (Plenum, New York, 1979).

[45] D. C. Clary, Mol. Phys. **44**, 1067 (1981); **44**, 1083 (1981); D. C. Clary and J. P. Henshaw, in *The Theory of Chemical Reaction Dynamics*, edited by D. C. Clary (Reidel, Dordrecht, 1986).

[46] V. Aquilanti, in *The Theory of Chemical Reaction Dynamics*, edited by D. C. Clary (Reidel, Dordrecht, 1986).